chemosensors

MDPI

Article

Antimonene-Modified Screen-Printed Carbon Nanofibers Electrode for Enhanced Electroanalytical Response of Metal Ions

María A. Tapia [1], Clara Pérez-Ràfols [1,2], Filipa M. Oliveira [3], Rui Gusmão [3,*], Núria Serrano [1,2,*], Zdeněk Sofer [3] and José Manuel Díaz-Cruz [1,2]

[1] Department of Chemical Engineering and Analytical Chemistry, Universitat de Barcelona (UB), Martí i Franquès 1-11, 08028 Barcelona, Spain; mtapia@ub.edu (M.A.T.); claraperezrafols@ub.edu (C.P.-R.); josemanuel.diaz@ub.edu (J.M.D.-C.)
[2] Water Research Institute (IdRA), Universitat de Barcelona (UB), Martí i Franquès 1-11, 08028 Barcelona, Spain
[3] Department of Inorganic Chemistry, University of Chemistry and Technology Prague, Technicka 5, 166 28 Prague, Czech Republic; filipa.oliveira@vscht.cz (F.M.O.); zdenek.sofer@vscht.cz (Z.S.)
* Correspondence: rui.gusmao@vscht.cz (R.G.); nuria.serrano@ub.edu (N.S.)

Abstract: A two-dimensional (2D) Sb-modified screen-printed carbon nanofibers electrode (2D Sb_{exf}-SPCNFE) was developed to improve the stripping voltammetric determination of Cd(II) and Pb(II), taking advantage of the synergistic effect between the two nanomaterials. The surface morphology of the 2D Sb_{exf}-SPCNFE was investigated by scanning electron microscopy, energy-dispersive X-ray spectroscopy, and Raman spectroscopy. The analytical performance of 2D Sb_{exf}-SPCNFE was compared to those presented by screen-printed carbon electrodes modified with 2D Sb_{exf} (2D Sb_{exf}-SPCE) and the corresponding bare electrodes: screen-printed carbon nanofibers electrode ($SPCNFE_{bare}$) and screen-printed carbon electrode ($SPCE_{bare}$). After optimizing the experimental conditions, the 2D Sb_{exf}-SPCNFE exhibited much better analytical parameters compared to the other assessed sensors. Analysis in 0.01 mol L^{-1} HCl (pH = 2) using 2D Sb_{exf}-SPCNFE showed excellent linear behavior in the concentration range of 2.9 to 85.0 μg L^{-1} and 0.3 to 82.0 μg L^{-1} for Cd(II) and Pb(II), respectively. The limits of detection after 240 s deposition time for Cd(II) and Pb(II) were 0.9 and 0.1 μg L^{-1}, and sensitivities between 1.5 and 3 times higher than those displayed by $SPCE_{bare}$, $SPCNFE_{bare}$, and 2D Sb_{exf}-SPCE were obtained. Finally, the 2D Sb_{exf}-SPCNFE was successfully applied to the determination of Cd(II) and Pb(II) traces in a certified estuarine water sample.

Keywords: antimonene; screen-printed electrodes; stripping voltammetry; carbon nanofibers; metal ions

Citation: Tapia, M.A.; Pérez-Ràfols, C.; Oliveira, F.M.; Gusmão, R.; Serrano, N.; Sofer, Z.; Díaz-Cruz, J.M. Antimonene-Modified Screen-Printed Carbon Nanofibers Electrode for Enhanced Electroanalytical Response of Metal Ions. *Chemosensors* **2023**, *11*, 219. https://doi.org/10.3390/chemosensors11040219

Academic Editors: Alessandro Silvestri and Alejandro Criado

Received: 24 February 2023
Revised: 27 March 2023
Accepted: 29 March 2023
Published: 1 April 2023

1. Introduction

Heavy metal water pollution is a significant environmental hazard that has detrimental consequences for organisms that are exposed to it, including plants, animals, and humans. Although heavy metal contamination of water can be due to both natural processes or anthropogenic activities, the main sources derive from industries, human dwellings, and agricultural activities that release substances into hydrological systems [1,2]. In terms of human health, some metal ions are essential and crucial for biological functions at low concentrations, but many other non-essential heavy metals are hazardous and have a long half-life that leads to the accumulation and contamination of food chains [3–5]. In fact, according to the ICH Q3D guidelines [6], metal ions such as arsenic, cadmium, mercury, and lead are considered Class 1 human toxicants. In particular, lead and cadmium are poisonous to humans, causing neurological, endocrine, hematological, renal, cardiovascular, respiratory, and skeletal disorders, miscarriages, and potentially presenting mutagenic and carcinogenic effects [7–9]. Cadmium and lead are hazardous at low concentrations, with the maximum limits established by the World Health Organization in drinking water being 3 μg L^{-1} and 10 μg L^{-1} for Cd(II) and Pb(II), respectively [2].

Heavy metals can be detected using several analytical techniques such as atomic fluorescence spectrometry (AFS) [10], graphite furnace atomic absorption spectrometry (GFAAS) [11], inductively coupled plasma mass spectrometry (ICP-MS) [12], inductively coupled plasma atomic emission spectrometry (ICP-AES) [13], and advance hyphenated techniques [6,14]. Although these techniques provide low detection limits and high sensitivity, the involved instruments are bulky and costly, and their handling requires skilled operators. In contrast, electroanalytical techniques based on the use of stripping voltammetry represent a powerful alternative to the former analytical techniques due to their fast, simple, selective, sensitive, and portable characteristics [7]. In this context, a wide range of sensors for the striping voltammetric determination of metal ions has been reported in the literature, including electrodes based on mercury, gold, carbon, bismuth, and antimony, among others [15,16]. However, over the past few decades, the manufacture of electrodes by screen-printing technology, which permits the mass fabrication of numerous highly reproducible, disposable, and low-cost screen-printed electrodes (SPEs), has attracted the attention of researchers as it allows to overcome the major drawbacks of solid electrodes. Moreover, the modification of the working electrode of SPEs with nanomaterials is trending because it can provide outstanding properties, such as high surface area, high electron transfer, adsorption capacity, and biocompatibility, thus improving the sensor's analytical performance [17,18]. In particular, it should be noted that electrodes based on carbon nanomaterials are being used nowadays not only for the determination of metal ions by themselves but also as a support to allow modifications that enhance their analytical performance [19–23].

In recent years, two-dimensional (2D) layered pnictogen materials, namely, phosphorene, arsenene, antimonene, and bismuthene, have arisen due to their exceptional physiochemical properties and functional structures. Liquid phase exfoliation has been extensively used to produce suspensions of many 2D materials mainly because it is the most suitable method to obtain few-layer sheets and it is suitable for industrial scale-up [24]. The amount of energy necessary to overcome the van der Waals forces between the layers of the bulk crystal is usually supplied in the form of ultrasonic waves or shear force. In fact, although some challenges occur for 2D materials that exhibit strong interlayer interactions with a greater covalent character, such as heavier pnictogens (rhombohedral Sb or Bi), there have still been reports on exfoliated pnictogen phases using these methods [25–27].

However, despite the remarkable characteristics of these emerging 2D-layered materials that make them suitable to be considered for the design of electrochemical sensors, the number of applications involving 2D-layered pnictogens for sensing is still scarce [26–34]. Nevertheless, the few reported applications show promising results. In recent work, bismuthene-based electrodes [27] and antimonene-based electrodes [26,30] demonstrated higher analytical performance for the determination of metal ions than those provided by classic bismuth- and antimony-based electrodes. Thus, the coupling of carbon nanomaterials with 2D-layered pnictogen nanomaterials appears as an attractive and innovative option to further improve the analytical performance of electrochemical sensors for the determination of metal ions. To the best of our knowledge, only a first approach based on the use of a hybrid bismuthene/graphene-modified glassy carbon electrode has been published by Lazanas *et al.* for the stripping voltammetric determination of Pb(II) and Cd(II) ions [31].

In this work, all aforementioned benefits have been considered in the development of an antimonene-modified electrode via drop-casting on a screen-printed carbon-based nanomaterial substrate leading to a 2D Sb-modified screen-printed carbon nanofibers electrode (2D Sb_{exf}-SPCNFE). On the one hand, antimonene is a 2D material composed of a single layer of antimony atoms in a rhombohedral structure that has received increasing attention in recent years due to its unique electronic and optical properties, making it a promising material for various applications, including energy storage, electronics, and sensing [34–36]. Among all 2D layered pnictogens, antimonene was selected because it has a direct band gap (i.e., it is more conductive and suitable for electronic applications) and

exhibits higher stability in a normal atmosphere, which makes it an appealing candidate for electrochemical sensing applications. Furthermore, antimonene has a high surface area compared to its bulk counterpart, gray antimony, which enhances its electrochemical performance [37]. On the other hand, an SPCNFE was chosen as an electrode platform as it was shown that for the development of a classic antimony film electrode, this support provided the best results in terms of sensitivity, repeatability, reproducibility, and detection limits for the determination of metal ions compared to other electrode platforms such as carbon screen-printed electrodes (SPCE), multi-walled carbon nanotubes modified screen-printed electrodes (SPCNTE) and graphene-modified screen-printed electrodes (SPGPE) [23]. The developed 2D Sb_{exf}-SPCNFE will be compared to a conventional screen-printed carbon-electrode-modified with 2D Sb_{exf} (2D Sb_{exf}-SPCE) and their respective bare electrodes (SPCNFE and SPCE) in terms of microscopic characterization and analytical performance in the simultaneous determination of Cd(II) and Pb(II) as a model metal ion system. Taking advantage of the superior analytical performance of 2D Sb_{exf}-SPCNFE, its applicability has been assessed through the simultaneous determination of Pb(II) and Cd(II) ions in a certified reference estuarine water sample.

2. Materials and Methods

2.1. Liquid-Phase Exfoliation of Gray Antimony

The liquid-phase exfoliation method of bulk gray rhombohedral antimony was adapted from our previously reported method [26] and is schematized in Scheme 1. For a fully detailed explanation of material exfoliation and characterization of the materials and sensors, the reader is referred to the Supplementary Material.

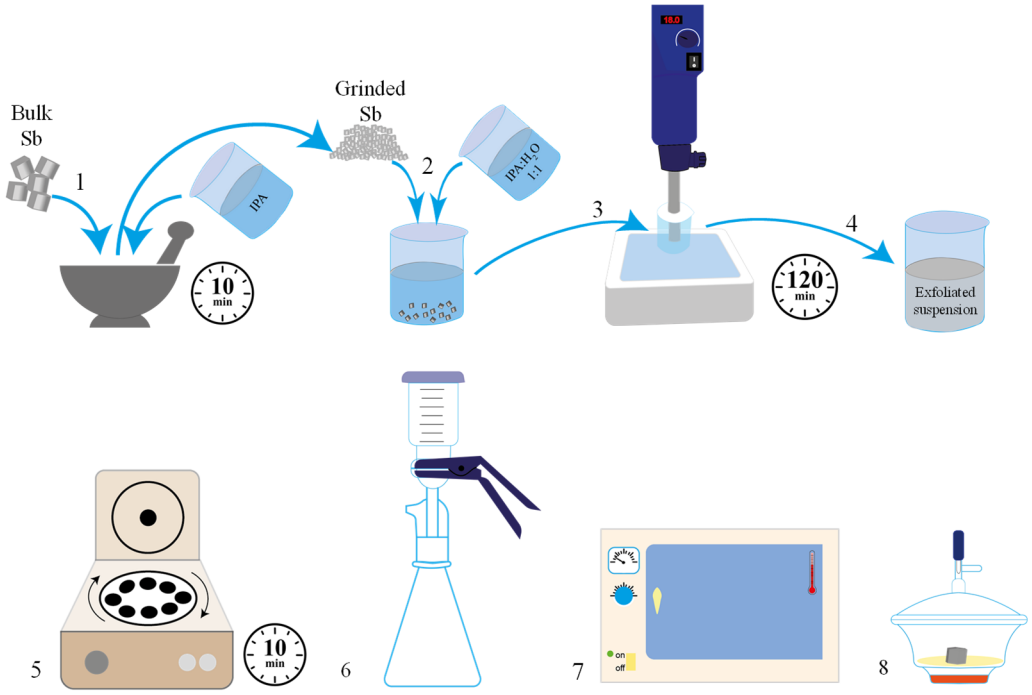

Scheme 1. Schematic figure of the liquid-phase exfoliation of gray antimony. (1) The bulk antimony and isopropanol were ground in an agate mortar; (2) ground antimony was added to 100 mL of IPA 1:1 H_2O; and (3) submitted to a high shear rate force; (4) the exfoliated suspension was (5) centrifuged, (6) filtered, (7) dried in the oven; and (8) stored under vacuum conditions.

2.2. Preparation of 2D Sb Modified Screen-Printed Electrodes

The accurate weight of the exfoliated layered antimony (antimonene) was suspended in deoxygenated water to obtain modifier suspensions at different concentrations: 0.75, 1.12, 2.50, and 5.00 mg mL^{-1}. The prepared suspensions were sonicated for 30 min while

keeping the temperature lower than 20 °C and then stored in the freezer until further use. The obtained suspensions could be stored for over one month without signs of degradation.

Unless otherwise indicated, 2D Sb-modified screen-printed carbon electrode (2D Sb_{exf}-SPCE) and 2D Sb-modified screen-printed carbon nanofibers electrode (2D Sb_{exf}-SPCNFE) were prepared as shown in Scheme 2, by drop-casting 5 µL of exfoliated antimony suspension (1.12 mg mL^{-1}) on the working electrode surface (4 mm diameter) of a carbon screen-printed electrode (SPCE) and a carbon nanofibers screen-printed electrode (SPCNFE) and drying them in the oven for 30 min at 25 °C.

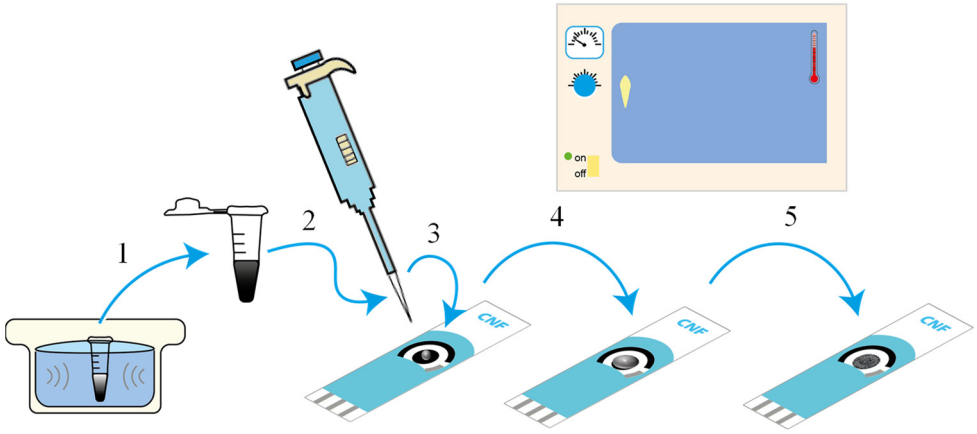

Scheme 2. Schematic figure of the preparation of 2D Sb-modified screen-printed electrodes. (1) sonicate the suspension; (2) pipette the 2D Sb suspension; (3) deposit the 2D Sb suspension on the working electrode; (4) evenly coat the working electrode; and (5) dry in the oven.

2.3. Voltammetric Measurements

All electrochemical measurements were carried out in a glass vessel at room temperature and without deaeration with a three-electrode configuration: Ag | AgCl | KCl (3 mol L^{-1}) as reference electrode, a platinum wire as a counter electrode, and a bare SPCE/SPCNFE or a modified SPCE/SPCNFE as working electrode.

DPASV measurements were conducted in 0.01 mol L^{-1} HCl (pH = 2) applying the following voltammetric parameters: deposition potential (E_d) of −1.4 V, deposition time (t_d) of 240 s with stirring, rest time (t_r) of 5 s, step potential of 8 mV, modulation time of 50 ms, pulse amplitude of 50 mV, and potential sweep ranging from −1.4 to −0.5 V. A conditioning/cleaning step was set before each DPASV measurement by applying −0.5 V for 30 s. Repeated scans of the blank solution were performed before starting the measurements until a constant baseline signal was achieved. A new bare or modified sensor unit was used for each set of measurements.

Calibration curves for the simultaneous DPASV determination of Pb(II) and Cd(II) were obtained by measuring increasing concentrations of the considered metal ions from 0.15 to about 130 µg L^{-1} using the following electrodes: $SPCE_{bare}$, $SPCNFE_{bare}$, 2D Sb_{exf}-SPCE, and 2D Sb_{exf}-SPCNFE at the above-described experimental conditions.

Certified estuarine water sample analysis was performed in triplicate following the standard addition method. For this purpose, a volume of the estuarine water sample was placed in the vessel with 0.01 mol L^{-1} HCl (pH = 2) (dilution factor 6/26), and the voltammogram was recorded at the above-established conditions. Then, three aliquots of Cd(II) and Pb(II) standard solutions were successively added, and the subsequent voltammograms were recorded.

3. Results and Discussion

3.1. Characterization

Scanning electron microscopy (SEM) was used to confirm the effective modification of the SPCE with 2D Sb and fibrillar carbon nanofibers (CNF). The as-received $SPCE_{bare}$

(Figure 1a) showed a surface predominantly composed of carbon (C), consistent with its role as a working electrode in which C is the active element. $SPCNFE_{bare}$ (Figure 1b) showed a surface that was better covered by C due to the presence of CNF, whereas in 2D Sb_{exf}-SPCE (Figure 1c), the distribution of bulk 2D Sb was visible. The SEM image of 2D Sb_{exf}-SPCNFE (Figure 1d) showed a good distribution of Sb within CNF, preserving the morphology of the starting materials. Elemental mapping of the materials was further evaluated using energy-dispersive X-ray spectroscopy (EDX). As expected, the EDX results (Figure S1) showed a higher carbon coverage of the electrode surface in $SPCNFE_{bare}$ (Figure S1b) than in $SPCE_{bare}$ (Figure S1a). Moreover, Sb distribution onto 2D Sb_{exf}-SPCE can be observed in Figure S1c and, with respect to 2D Sb_{exf}-SPCNFE (Figure S1d), both Sb and C were well-distributed and present in the sample, indicating that the 2D Sb_{exf}-SPCNFE sample had a well-balanced elemental composition.

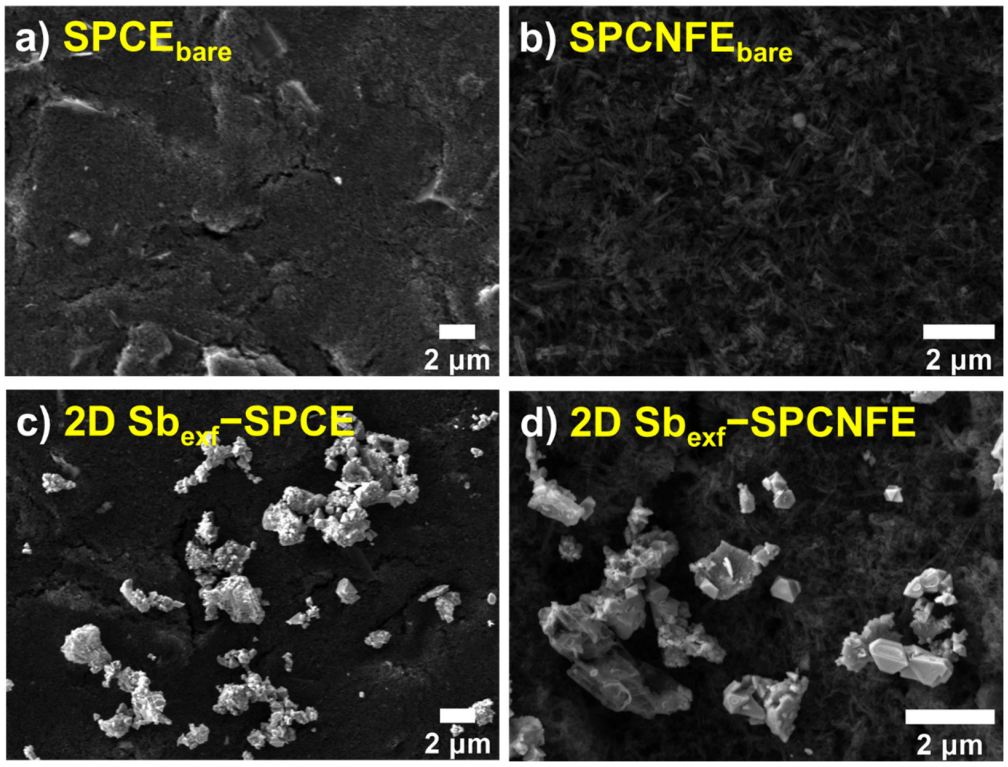

Figure 1. SEM micrographs of (**a**) $SPCE_{bare}$, (**b**) $SPCNFE_{bare}$, (**c**) 2D Sb_{exf}-SPCE, and (**d**) 2D Sb_{exf}-SPCNFE.

The Raman spectroscopy characterization of the studied samples (Figure 2a) presented differences in their vibrations and structural characteristics. The $SPCNFE_{bare}$ sample showed the typical D- and G-bands of carbon structures, and the 2D Sb_{exf}-SPCE sample exhibited the phonon frequencies of the E_g and A_{1g} modes related to 2D Sb at 112.2 and 150.0 cm^{-1} (Figure S2), respectively [9]. These frequencies were in agreement with those observed for the starting gray-Sb (Figure S2) and were also observed at 109.6 and 150.0 cm^{-1} in the Raman spectrum of 2D Sb_{exf}-SPCNFE, which also presented D- and G-bands at 1340.7 and 1574.2 cm^{-1}, respectively. For easier inspection, a more detailed spectrum of 2D Sb_{exf}-SPCNFE is shown in Figure 2b. Overall, these results show that there is a well-integrated combination of Sb and CNF in the 2D Sb_{exf}-SPCNFE sample.

TEM characterization was performed to confirm that the bulk Sb was effectively converted into 2D Sb_{exf} through the liquid exfoliation process (Figure S3). The TEM micrograph in Figure S3a shows a representative view of the few-layered 2D Sb_{exf} with well-defined regular lattice fringes (Figure S3b) with a lattice spacing of 0.313 and 0.315 nm. The selected area electron diffraction (SAED) pattern (Figure S3c) indicates that the Sb_{exf} is crystalline

with a rhombohedral lattice. The STEM micrograph in Figure S3d shows the elemental mapping, which confirms a homogeneous distribution of Sb on the material surface.

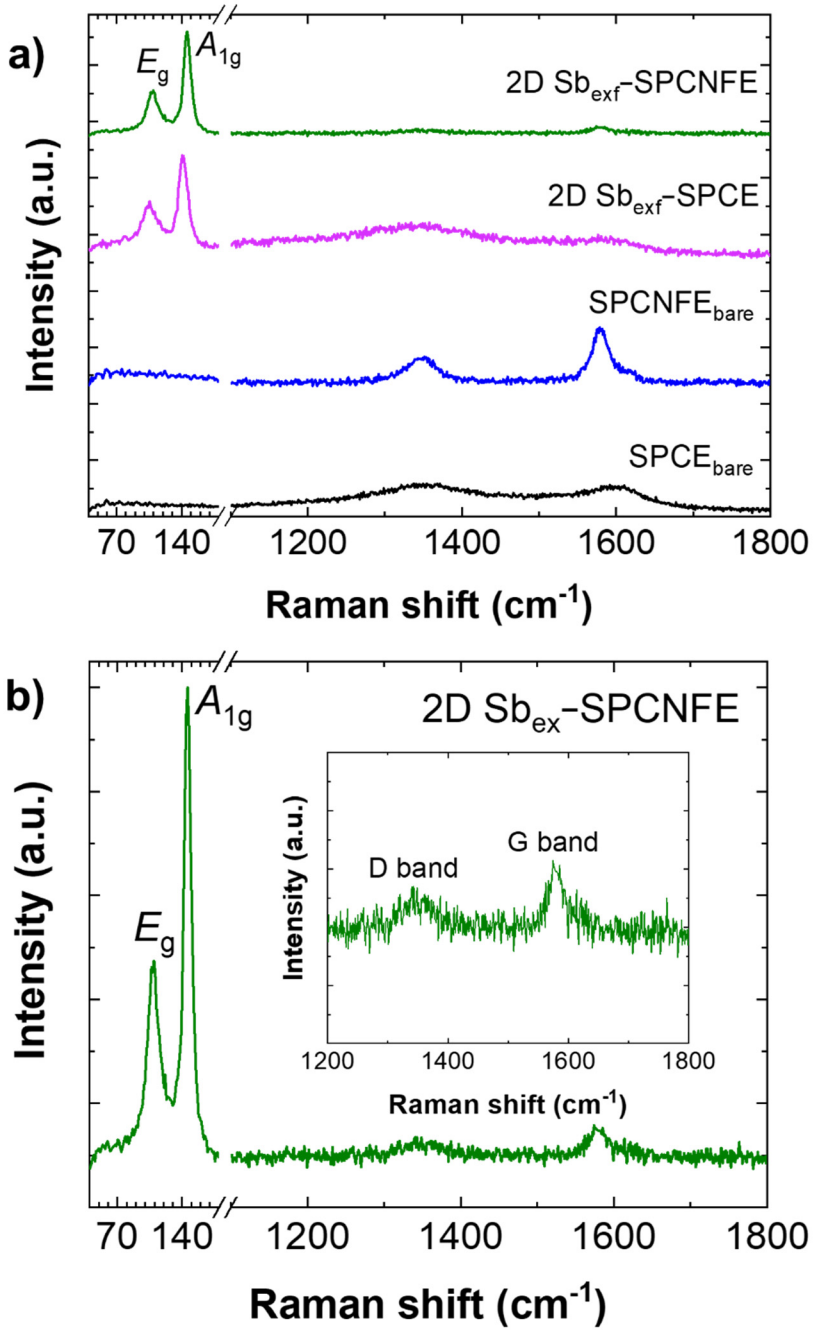

Figure 2. (**a**) Raman spectra of 2D Sb_{exf}−SPCNFE compared to other modified SPCEs with the representation of phonon frequencies of the E_g and A_{1g} modes characteristic of antimony. (**b**) Detail of the Raman spectrum of 2D Sb_{ex}−SPCNFE with an inset showing the D− and G−bands.

3.2. Differential Pulse Anodic Stripping Voltammetry (DPASV) of Cd (II) and Pb (II)

The DPASV response corresponding to the determination of Cd(II) and Pb(II) using a 2D Sb_{exf}-SPCNFE was assessed and then compared to those provided by 2D Sb_{exf}-SPCE and their respective bare electrodes (SPCE and SPCNFE).

First, the experimental conditions for the DPASV determination of Cd(II) and Pb(II) were optimized using 2D Sb_{exf}-SPCNFE. 0.01 mol L^{-1} hydrochloric acid (pH = 2) and acetate buffer 0.1 mol L^{-1} (pH = 4.5) were evaluated for the determination of Pb(II) and Cd(II) using

2D Sb_{exf}-SPCNFE. Hydrochloric acid 0.01 mol L^{-1} (pH = 2) was selected as the optimal supporting electrolyte since it provided better-defined peaks for Cd(II) and Pb(II) compared to those attained using acetate buffer (pH = 4.5), especially at lower concentrations.

Deposition potential (E_d) and deposition time (t_d) were evaluated considering ranges from −0.9 V to −1.4 V and from 30 s to 240 s, respectively, in a solution containing 50 µg L^{-1} Cd(II) and Pb(II) in hydrochloric acid 0.01 mol L^{-1} (pH = 2) and using a 2D Sb_{exf}-SPCNFE prepared from a 2D Sb_{exf} suspension of 1.12 mg mL^{-1}. The selected compromise conditions were an E_d of −1.4 V, applied with stirring during a t_d of 240 s.

Once the voltammetric conditions were established, the concentration of the exfoliated layered antimony (antimonene, 2D Sb_{exf}) suspension employed in the drop-casting procedure was optimized. In the case of 2D Sb_{exf}-SPCE, it was reported in a previous work that the best voltammetric response was achieved by depositing a 5 µL drop of 1.12 mg mL^{-1} 2D Sb_{exf} suspension on the SPCE surface [26] and therefore, this concentration was considered optimal. Nevertheless, this value cannot directly be assumed as optimal for 2D Sb_{exf}-SPCNFE because, as seen in the previous section, the morphological characteristics of the substrate are different and could influence the drop-casting of the 2D Sb_{exf} suspension. Therefore, different SPCNFE units were modified with 2D Sb_{exf} suspensions of four different concentrations (0.75, 1.12, 2.50, and 5.00 mg mL^{-1}) following the modification protocol established in Section 2.2 and simultaneous voltammetric measurements of a solution containing 20 µg L^{-1} of Cd(II) and Pb(II) were performed with each 2D Sb_{exf} based- SPCNFE. As shown in Figure 3, the highest and best-defined Cd(II) and Pb(II) voltammetric peaks were obtained by modifying the SPCNFE with 1.12 mg mL^{-1} 2D Sb_{exf} suspension. Therefore, for both 2D Sb_{exf}-SPCE and 2D Sb_{exf}-SPCNFE, the 2D Sb_{exf} suspension of 1.12 mg mL^{-1} was considered for further modification procedures.

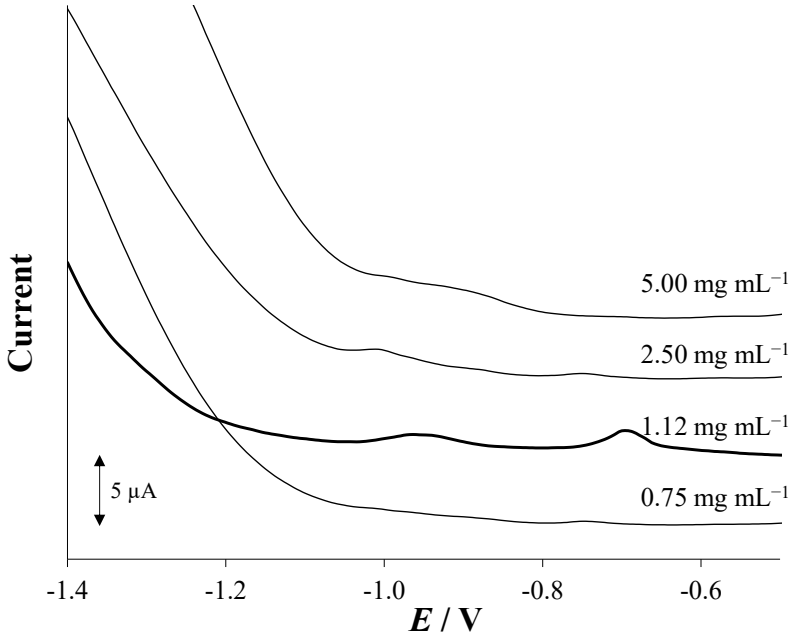

Figure 3. Effect of the concentration of the 2D Sb_{exf} suspension drop-casted on the surface of the working electrode of the SPCNFE on the DP stripping voltammograms for 20 µg L^{-1} of Cd(II) and Pb(II). Electrochemical measurements were carried out at pH 2, E_d of −1.4 V, and t_d of 240 s.

Once the concentration of the modifier suspension was optimized, the electroanalytical performance of 2D Sb_{exf}-SPCNFE was studied in terms of sensitivity, linear range, the limit of detection (LOD), and the limit of quantification (LOQ). For this purpose, calibration curves were carried out for the simultaneous determination of Cd(II) and Pb(II) ions in 0.01 mol L^{-1} HCl (pH = 2). DP stripping voltammograms were recorded with 2D Sb_{exf}-SPCNFE at the above-stated experimental conditions using sequential additions of

metal ions within a range of concentrations between 0.05 and 130 μg L^{-1}, as shown in Figure 4. Well-shaped voltammetric peaks appeared at *ca.* −0.95 and −0.70 V for different concentrations of Cd(II) and Pb(II) ions, respectively, as shown in Figure 4A. The analytical parameters calculated are summarized in Table 1. The results revealed that there was a good linear relationship up to a concentration of *ca.* 85 μg L^{-1} with a regression coefficient (R^2) of 0.999 for both metal ions (Figure 4B). The sensitivity established from the slope of the calibration plots was 6.19 (0.05) and 6.597 (0.008) nA V μg^{-1} L for Cd(II) and Pb(II) ions, respectively. LODs were calculated as 0.9 and 0.1 μg L^{-1}, and LOQs were calculated as 2.9 and 0.3 for Cd(II) and Pb(II), respectively, using the equation '3 σ/s' for LOD and '10 σ/s' for the LOQ (where 'σ' is the standard deviation of the intercept and 's' is the slope of the calibration plot). This finding indicates that there is a high sensitivity of the novel 2D Sb_{exf}-SPCNFE regarding the determination of Cd(II) and Pb(II) ions.

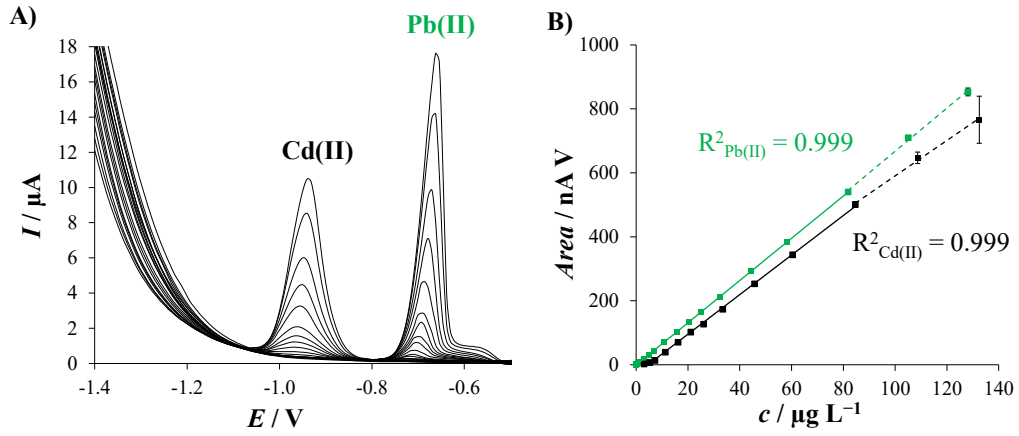

Figure 4. (**A**) DPASV responses of 2D Sb_{exf}-SPCNFE for the simultaneous determination of increasing concentrations of Pb(II) and Cd(II) ions at pH 2, E_d of −1.4 V and t_d of 240 s; and (**B**) corresponding calibration curves. Solid lines indicate the data used to calculate the linear ranges. Three replicates were considered to calculate the error bars.

Table 1. Comparison of the analytical performance of $SPCE_{bare}$, $SPCNFE_{bare}$, 2D Sb_{exf}-SPCE, and 2D Sb_{exf}-SPCNFE for the simultaneous determination of Pb(II) and Cd(II) by DPASV at pH 2, E_d of −1.4 V and t_d of 240 s. The standard deviations are shown within brackets.

	$SPCE_{bare}$		$SPCNFE_{bare}$		2D Sb_{exf}-SPCE		2D Sb_{exf}-SPCNFE	
	Cd(II)	**Pb(II)**	**Cd(II)**	**Pb(II)**	**Cd(II)**	**Pb(II)**	**Cd(II)**	**Pb(II)**
Sensitivity (nA V μg^{-1} L)	2.9 (0.1)	2.6 (0.1)	4.69 (0.09)	5.6 (0.1)	4.09 (0.06)	4.50 (0.01)	6.19 (0.05)	6.597 (0.008)
Intercept (μg L^{-1})	−62 (6)	−1 (1)	−59 (5)	−36 (5)	−12 (4)	−0.5 (0.5)	−28 (2)	−0.1 (0.2)
1st Linear range (μg L^{-1}) [a]	20.3–104.5	6.9–29.6	10.8–108.7	9.8–105.1	9.1–132.7	1.1–128.3	2.9–85.0	0.3–82.0
R^2	0.987	0.980	0.994	0.993	0.994	0.999	0.999	0.999
2nd Linear range (μg L^{-1}) [a]	-	29.6–101.1	-	-	-	-	-	-
R^2		0.988						
LOD (μg L^{-1})	6.1	2.1	3.2	2.9	2.7	0.3	0.9	0.1

[a] The lowest value of the linear range was calculated from the LOQ.

The analytical performance obtained for 2D Sb_{exf}-SPCNFE was compared with those achieved by Sb_{exf}-SPCE and their corresponding bare electrodes (*i.e.*, SPCE and SPCNFE). Figure 5 compares the DPASV responses for 55 μg L^{-1} Pb(II) and Cd(II) in HCl 0.01 mol L^{-1} (pH = 2) recorded using $SPCE_{bare}$, $SPCNFE_{bare}$, 2D Sb_{exf}-SPCE, and 2D Sb_{exf}-SPCNFE. As expected, the bare electrodes provided the lowest voltammetric peaks, being the Cd(II) and Pb(II) peaks attained by $SPCNFE_{bare}$, which were higher than those obtained by $SPCE_{bare}$, particularly in the case of Cd(II). This is due to the increased effective surface area and improved electron-transfer kinetics provided by the presence of CNF. By comparing the DPASV voltammograms obtained by $SPCNFE_{bare}$ and 2D Sb_{exf}-SPCE, it can be concluded

that a slightly larger response was accomplished by the modification with 2D Sb_{exf} instead of using CNF as a modifier. However, the highest and most well-defined Cd(II) and Pb(II) peaks were achieved by Sb_{exf}-SPCNFE, in which the excellent properties of both nanomaterials were merged. These findings are supported by the analytical parameters summarized in Table 1. As can be seen in Table 1, the sensitivity provided by 2D Sb_{exf}-SPCNFE was between 1.2 and 2.5 times higher, depending on the considered metal ion, than those provided by $SPCE_{bare}$, $SPCNFE_{bare}$, and 2D Sb_{exf}-SPCE, while still maintaining a reasonably linear range. However, it should be noted that CNF-based sensors yield higher sensitivity than those based on carbon. Regarding the LODs, the lowest LODs were also achieved using 2D Sb_{exf}-SPCNFE, whose values were between 3 and 29 times lower, depending on the considered metal ion, than those attained by the other assessed sensors. On the view of the obtained results, it can be concluded that the excellent analytical performance exhibited by 2D Sb_{exf}-SPCNFE can be attributed to a synergistic effect between both nanomaterials: the high electrical conductivity and large surface area provided by CNF together with the high surface volume ratio and the high charge carrier mobility added by 2D Sb_{exf}.

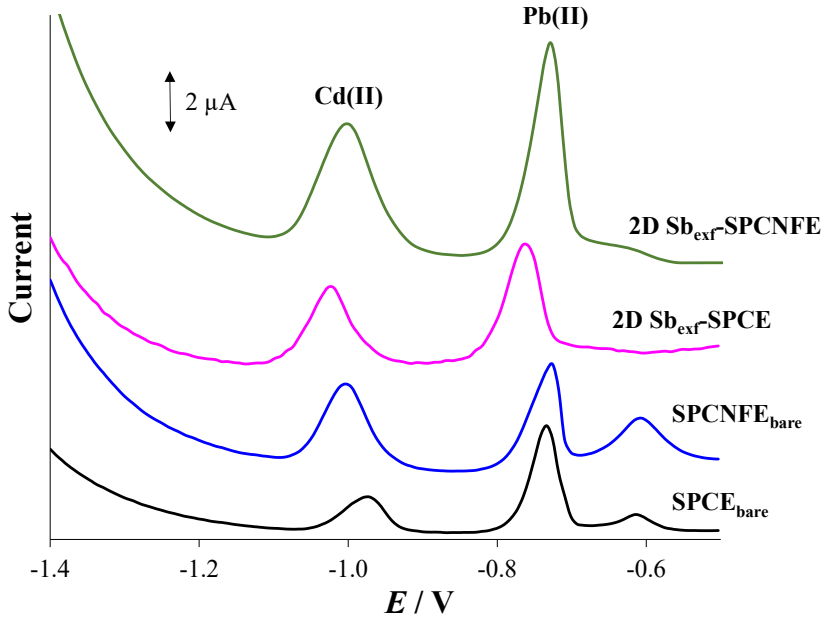

Figure 5. DP stripping voltammograms of 55 µg L^{-1} of Cd(II) and Pb(II) were recorded at pH 2 applying an E_d of −1.4 V for 240 s using $SPCE_{bare}$, $SPCNFE_{bare}$, 2D Sb_{exf}-SPCE, and 2D Sb_{exf}-SPCNFE.

The repeatability of 2D Sb_{exf}-SPCNFE was evaluated under optimized conditions using 25 µg L^{-1} of Cd(II) and Pb(II). Five repetitive measurements were made using the same 2D Sb_{exf}-SPCNFE unit. The calculated relative standard deviations (RSD) were 1.7% and 1.3% for Cd(II) and Pb(II), respectively. Moreover, the reproducibility study of the 2D Sb_{exf}-SPCNFE involved the preparation of three 2D Sb_{exf}-SPCNFE units, which were then applied to the determination of 25 µg L^{-1} of Cd(II) and Pb(II). The RSDs of 2D Sb_{exf}-SPCNFE were 6.9% and 2.7% for Cd(II) and Pb(II), respectively. These results indicated that the developed 2D Sb_{exf}-SPCNFE showed great repeatability and reproducibility, similar to those achieved by 2D Sb_{exf}-SPCE [26].

Regarding the previous findings, it should be noted that, to the best of our knowledge, apart from the above-discussed approach based on the use of 2D Sb_{exf}-SPCE [26], there are no more works dealing with the use of antimonene or 2D Sb_{exf} for the voltammetric determination of metal ions. Compared to other developed electrodes based on the use of antimony and carbon nanomaterials for the simultaneous determination of Cd(II) and Pb(II) (Table S1), the developed 2D Sb_{exf}-SPCNFE provides, in general terms, better analytical parameters [15,22,23,38,39]. For example, the LODs obtained by an antimony nanoparticle-

multiwalled carbon nanotubes composite immobilized on a carbon paste electrode were 0.77 μg L^{-1} for Cd(II) and 0.65 μg L^{-1} for Pb(II) [22]. Much higher LODs were also achieved, for example, by an antimony film electrode prepared from CNF modified screen-printed electrode (2.1 and 1.1 μg L^{-1} for Cd(II) and Pb(II), respectively) [23], by a graphene oxide-modified GC electrode coated with in situ antimony film (6.07 and 5.39 μg L^{-1} for Cd(II) and Pb(II), respectively) [38], and by a multiwall carbon nanotube modified by antimony oxide–carbon paste electrode (16.77 and 6.12 μg L^{-1} for Cd(II) and Pb(II), respectively) [39]. Compared to the LODs obtained by the hybrid bismuthene/graphene-modified GC electrode (0.3 μg L^{-1} for both Cd(II) and Pb(II)) [31], 2D Sb_{exf}-SPCE provided a better LOD for Pb(II) and a somewhat higher LOD for Cd(II). Moreover, it should be underlined that the developed 2D Sb_{exf}-SPCNFE has advantages, such as the relatively higher stability in the normal atmosphere of 2D Sb_{exf}, the easy and very fast modification procedure based on the drop-casting approach, and the use of low-cost, disposable and reproducible platforms. On the other hand, the durability of the 2D Sb_{exf} immobilization on every screen-printed platform for a large set of measurements (more than 20) without loss of sensitivity enables the voltammetric determination of metal ions with the same 2D Sb_{exf}-SPCNFE unit.

3.3. Analysis of an Estuarine Water Sample Using a 2D Sb_{exf}-SPCNFE

A certified estuarine water reference material (LGC6016) was chosen to evaluate the feasibility of a 2D Sb_{exf}-SPCNFE sensor for the simultaneous determination of Cd(II) and Pb(II) in a natural water sample. The determination of the studied metal ions was performed by the standard addition method. Then, DPASV measurements, including the analyzed sample and three additions of Cd(II) and Pb(II), were conducted in triplicate at the above-stated conditions. Figure 6A shows representative voltammograms with very well-defined peaks for both metal ions attained in the analysis of the estuarine water samples using 2D Sb_{exf}-SPCNFE. Figure 6B illustrates the calibration plot for Cd(II) and Pb(II) with a notorious correlation between peak areas and the added concentrations for both considered metal ions.

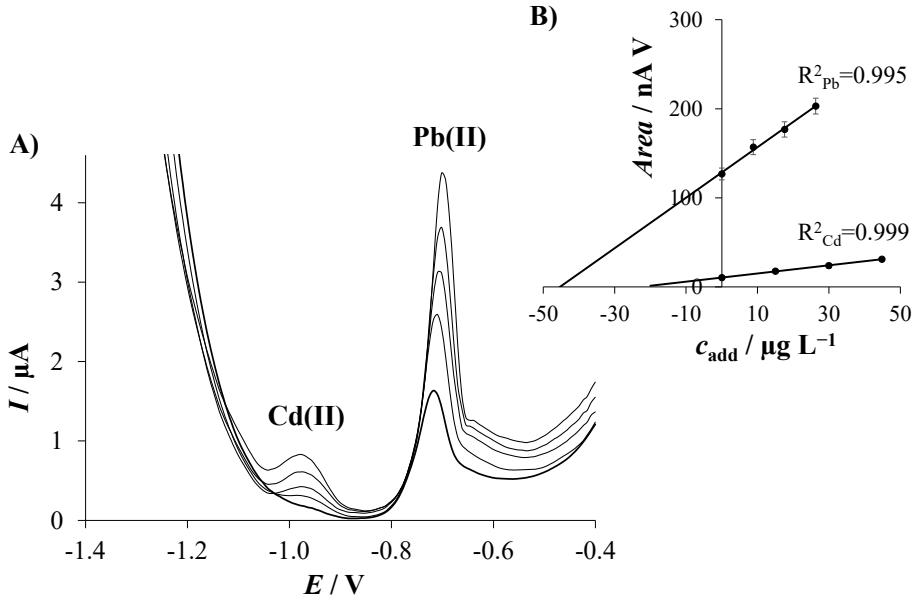

Figure 6. (**A**) Stripping voltammograms for simultaneous determination of Cd(II) and Pb(II) ions in a certified estuarine water reference material sample using 2D Sb_{exf}-SPCNFE at pH 2, E_d of −1.4 V, and t_d of 240 s; and (**B**) linear regression plots of the standard addition measurements.

Table 2 reports the Cd(II) and Pb(II) concentration data obtained from the DP stripping voltammetric analysis of three replicates of the estuarine water sample performed using the 2D Sb_{exf}-SPCNFE. An outstanding agreement was attained between all replicates as

well as with the Cd(II)- and Pb(II)-certified values provided in the estuarine water reference material sample. Furthermore, it should be highlighted that the certified estuarine water sample contains more constituents, such as Cu, Mn, Ni, Ca, Mg, K, Na, and Zn, which did not disturb the determination of Cd(II) and Pb(II) in the sample.

Table 2. Simultaneous determination of Pb(II) and Cd(II) by DPASV in a certified estuarine water sample (LGC6016) on 2D Sb_{exf}-SPCNFE at pH 2, E_d of −1.4 V, and t_d 240 s.

	Cd(II)			Pb(II)		
	c (μg L^{-1})	RSD[a] (%)	Relative Error (%)	c (μg L^{-1})	RSD[a] (%)	Relative Error (%)
2D Sb_{exf}-SPCNFE	99.1	3.18	1.88	196.3	2.52	0.17
Certified metal value	101.0	2.00	-	196.0	1.50	-

[a] n = 3 was considered for RSD (%) calculation.

Considering the excellent reproducibility and trueness achieved in the simultaneous determination of Cd(II) and Pb(II) ions in the estuarine water sample, we can state that the developed sensor based on the combination of two nanomaterials (CNF and 2D Sb_{exf}) is fully suitable for voltammetric stripping measurements of metal ions at low trace levels in real water sample levels, even in the presence of other elements at similar or higher concentrations than Pb(II) and Cd(II).

4. Conclusions

A 2D Sb_{exf}-SPCNFE was developed for the simultaneous DPASV determination of Pb(II) and Cd(II) as a model metal ion system and morphologically characterized by SEM, EDX, and Raman spectroscopy. The developed 2D Sb_{exf}-SPCNFE takes advantage of the merging of antimonene (2D Sb_{exf}) and CNF within the same platform. 2D Sb_{exf}-SPCNFE showed well-defined and separated stripping peaks for Cd(II) and Pb(II) with great repeatability and reproducibility. The analytical performance provided by 2D Sb_{exf}-SPCNFE was much better than those achieved by 2D Sb_{exf}-SPCE and the respective bare electrodes (SPCNFE and SPCE) in terms of linear range, LODs, LOQs, and sensitivities. Compared to other reported sensors based on the use of antimony and carbon nanomaterials, the analytical parameters exhibited by 2D Sb_{exf}-SPCNFE were also generally superior. The excellent analytical performance demonstrated by 2D Sb_{exf}-SPCNFE can be associated with a synergistic effect between the excellent properties attributed to both merged nanomaterials, i.e., the high surface-volume ratio and the high charge carrier mobility provided by 2D Sb_{exf}, and the high electrical conductivity and the large surface area added using CNF.

The applicability of the developed sensor was evaluated by detecting trace levels of Pb(II) and Cd(II) in a certified reference estuarine water sample, obtaining good reproducibility and trueness without the interference of constituents at similar or higher concentrations than Pb(II) and Cd(II).

Thus, the remarkable analytical performance displayed by 2D Sb_{exf}-SPCNFE coupled with the simple modification procedure involved and the use of low-cost, disposable, and reproducible platforms suggests that 2D Sb_{exf}-SPCNFE is a great alternative to other reported sensors for the voltammetric determination of metal ions in environmental samples.

Supplementary Materials: The following supporting information can be downloaded at: https://www.mdpi.com/article/10.3390/chemosensors11040219/s1. Materials and Methods: reagents and solutions; electrochemical instrumentation; liquid-phase exfoliation of gray antimony; and characterization of materials and electrodes. Figures: Figure S1. EDX elemental mapping of elements in (a) $SPCE_{bare}$, (b) $SPCNFE_{bare}$, (c) 2D Sb_{exf}-SPCE, and (d) 2D Sb_{exf}-SPCNFE; Figure S2. Raman spectrum of pure bulk antimony with the representation of phonon frequencies of the E_g and A_{1g} modes at 112.2 and 150.0 cm^{-1}, respectively. Figure S3. Characterization of 2D Sb_{exf}: (a) TEM and (b) HRTEM images with a detail showing well-defined layered phases in 2D Sb_{exf}. (c) SAED pattern. (d) STEM image with inset of mapping of Sb element. Scale bars represent 1 μm in STEM and EDX images. Tables: Table S1. Summary of various electrodes based on the use of antimony and carbon

nanomaterials, and the hybrid bismuthene/graphene-modified GC electrode for the determination of Cd(II) and Pb(II).

Author Contributions: Conceptualization: N.S. and R.G.; Methodology: M.A.T., C.P.-R., R.G., N.S., Z.S. and J.M.D.-C.; Formal analysis: M.A.T., F.M.O., C.P.-R., R.G. and N.S.; Investigation: M.A.T., F.M.O., C.P.-R., R.G. and N.S.; Visualization: C.P.-R., R.G., N.S., J.M.D.-C. and Z.S.; Validation: J.M.D.-C.; Writing–original draft: N.S. and R.G.; Writing–review & editing: C.P.-R., M.A.T., F.M.O., Z.S. and J.M.D.-C.; Resources: C.P.-R., R.G., N.S., J.M.D.-C. and Z.S. All authors have read and agreed to the published version of the manuscript.

Funding: This work is supported by PID2019-107102RB-C22 funded by MCIN/AEI/10.13039/501100011033, and Project GACR No 19-26910X funded by the Czech Science Foundation.

Institutional Review Board Statement: Not applicable.

Informed Consent Statement: Not applicable.

Data Availability Statement: Not applicable.

Acknowledgments: The authors thankfully acknowledge the support of the Generalitat of Catalunya, Spain (project 2021 SGR 00006). Maria Tapia acknowledges the support of the Water Research Institute (IdRA) of the University of Barcelona and the support of the Peruvian National Program of Scholarships and Student Loans (PRONABEC) for her Ph.D. grant (Beca Presidente de la República–343245). F.M.O. acknowledges the European Structural and Investment Funds, CHEMFELLS V (No. CZ.02.01.01/00/22_010/0003004). This research was also supported by GAČR No 19-26910X funded by the Czech Science Foundation.

Conflicts of Interest: The authors declare no conflict of interest that could influence the work reported in this paper. The funders had no role in the design of the study; in the collection, analyses, or interpretation of data; in the writing of the manuscript; nor in the decision to publish the results.

References

1. Sall, M.L.; Diaw, A.K.D.; Gningue-Sall, D.; Efremova Aaron, S.; Aaron, J.J. Toxic heavy metals: Impact on the environment and human health, and treatment with conducting organic polymers, a review. *Environ. Sci. Pollut. Res.* **2020**, *27*, 29927–29942. [CrossRef] [PubMed]
2. World Health Organization. *Guidelines for Drinking-Water Quality*, 4th ed.; World Health Organization: Geneva, Switzerland, 2017; ISBN 9789241549950.
3. Raj, D.; Maiti, S.K. Sources, bioaccumulation, health risks and remediation of potentially toxic metal(loid)s (As, Cd, Cr, Pb and Hg): An epitomised review. *Environ. Monit. Assess.* **2020**, *192*, 108. [CrossRef]
4. Ali, H.; Khan, E.; Ilahi, I. Environmental chemistry and ecotoxicology of hazardous heavy metals: Environmental persistence, toxicity, and bioaccumulation. *J. Chem.* **2019**, *2019*, 6730305. [CrossRef]
5. Ravipati, E.S.; Mahajan, N.N.; Sharma, S.; Hatware, K.V.; Patil, K. The toxicological effects of lead and its analytical trends: An update from 2000 to 2018. *Crit. Rev. Anal. Chem.* **2021**, *51*, 87–102. [CrossRef] [PubMed]
6. ICH Expert Working Group ICH harmonised guideline, Guideline for elemental impurities Q3D (R1). *ICH Guidel. Q3D Elem. Impurities* **2019**.
7. Wang, J. *Stripping Analysis: Principles, Instrumentation and Applications*; VCH: Deerfield Beach, FL, USA, 1985.
8. Kaur, M.; Sharma, P.; Kaur, R.; Khetarpal, P. Increased incidence of spontaneous abortions on exposure to cadmium and lead: A systematic review and meta-analysis. *Gynecol. Endocrinol.* **2022**, *38*, 16–21. [CrossRef]
9. Genchi, G.; Sinicropi, M.S.; Graziantono, L.; Carocci, A.; Catalano, A. The effects of Cadmium toxicity. *Int. J. Environ. Res. Public Health* **2020**, *17*, 3782. [CrossRef]
10. Chen, Y.; Li, M.; Fu, L.; Hou, X.; Jiang, X. Simultaneous determination of trace cadmium and lead in single human hair by tungsten electrothermal vaporization-flame atomic fluorescence spectrometry. *Microchem. J.* **2014**, *114*, 182–186. [CrossRef]
11. Valasques, G.S.; dos Santos, A.M.P.; de Souza, V.S.; Teixeira, L.S.G.; Alves, J.P.S.; de Jesus Santos, M.; dos Santos, W.P.C.; Bezerra, M.A. Multivariate optimization for the determination of cadmium and lead in crude palm oil by graphite furnace atomic absorption spectrometry after extraction induced by emulsion breaking. *Microchem. J.* **2020**, *153*, 104401. [CrossRef]
12. Wysocka, I.; Vassileva, E. Determination of cadmium, copper, mercury, lead and zinc mass fractions in marine sediment by isotope dilution inductively coupled plasma mass spectrometry applied as a reference method. *Microchem. J.* **2016**, *128*, 198–207. [CrossRef]
13. Roje, V.; Galinec, F. Water as a mild extractant of metals and metalloids from the samples of the selected certified reference materials and subsequent multi-elemental quantification by ICP-AES. *Environ. Monit. Assess.* **2019**, *191*, 534. [CrossRef]
14. Barałkiewicz, D.; Kózka, M.; Piechalak, A.; Tomaszewska, B.; Sobczak, P. Determination of cadmium and lead species and phytochelatins in pea (Pisum sativum) by HPLC-ICP-MS and HPLC-ESI-MSn. *Talanta* **2009**, *79*, 493–498. [CrossRef]

15. Ariño, C.; Serrano, N.; Díaz-Cruz, J.M.; Esteban, M. Voltammetric determination of metal ions beyond mercury electrodes. A review. *Anal. Chim. Acta* **2017**, *990*, 11–53. [CrossRef] [PubMed]
16. Martín-Yerga, D.; González-García, M.B.; Costa-García, A. Electrochemical determination of mercury: A review. *Talanta* **2013**, *116*, 1091–1104. [CrossRef] [PubMed]
17. Chu, Z.; Peng, J.; Jin, W. Advanced nanomaterial inks for screen-printed chemical sensors. *Sens. Actuators B Chem.* **2017**, *243*, 919–926. [CrossRef]
18. Tyagi, D.; Wang, H.; Huang, W.; Hu, L.; Tang, Y.; Guo, Z.; Ouyang, Z.; Zhang, H. Recent advances in two-dimensional-material-based sensing technology toward health and environmental monitoring applications. *Nanoscale* **2020**, *12*, 3535–3559. [CrossRef]
19. Pérez-Ràfols, C.; Serrano, N.; Díaz-Cruz, J.M.; Ariño, C.; Esteban, M. Glutathione modified screen-printed carbon nanofiber electrode for the voltammetric determination of metal ions in natural samples. *Talanta* **2016**, *155*, 8–13. [CrossRef]
20. Zhang, B.; Chen, J.; Zhu, H.; Yang, T.; Zou, M.; Zhang, M.; Du, M. Facile and green fabrication of size-controlled AuNPs/CNFs hybrids for the highly sensitive simultaneous detection of heavy metal ions. *Electrochim. Acta* **2016**, *196*, 422–430. [CrossRef]
21. Gao, S.; Xu, C.; Yalikun, N.; Mamat, X.; Li, Y.; Wågberg, T.; Hu, X.; Liu, J.; Luo, J.; Hu, G. Sensitive and Selective Differential Pulse Voltammetry Detection of Cd(II) and Pb(II) Using Nitrogen-Doped Porous Carbon Nanofiber Film Electrode. *J. Electrochem. Soc.* **2017**, *164*, H967–H974. [CrossRef]
22. Ashrafi, A.M.; Cerovac, S.; Mudrić, S.; Guzsvány, V.; Husáková, L.; Urbanová, I.; Vytřas, K. Antimony nanoparticle-multiwalled carbon nanotubes composite immobilized at carbon paste electrode for determination of trace heavy metals. *Sens. Actuators B Chem.* **2014**, *191*, 320–325. [CrossRef]
23. Pérez-Ràfols, C.; Serrano, N.; Díaz-Cruz, J.M.; Ariño, C.; Esteban, M. New approaches to antimony film screen-printed electrodes using carbon-based nanomaterials substrates. *Anal. Chim. Acta* **2016**, *916*, 17–23. [CrossRef] [PubMed]
24. Gibaja, C.; Rodriguez-San-Miguel, D.; Ares, P.; Gómez-Herrero, J.; Varela, M.; Gillen, R.; Maultzsch, J.; Hauke, F.; Hirsch, A.; Abellán, G.; et al. Few-layer antimonene by liquid-phase exfoliation. *Angew. Chemie Int. Ed.* **2016**, *55*, 14345–14349. [CrossRef] [PubMed]
25. Gibaja, C.; Assebban, M.; Torres, I.; Fickert, M.; Sanchis-Gual, R.; Brotons, I.; Paz, W.S.; Palacios, J.J.; Michel, E.G.; Abellán, G.; et al. Liquid phase exfoliation of antimonene: Systematic optimization, characterization and electrocatalytic properties. *J. Mater. Chem. A* **2019**, *7*, 22475–22486. [CrossRef]
26. Tapia, M.A.; Pérez-Ràfols, C.; Paštika, J.; Gusmão, R.; Serrano, N.; Sofer, Z.; Díaz-Cruz, J.M. Antimony nanomaterials modified screen-printed electrodes for the voltammetric determination of metal ions. *Electrochim. Acta* **2022**, *425*, 140690. [CrossRef]
27. Tapia, M.A.; Pérez-Ràfols, C.; Gusmão, R.; Serrano, N.; Sofer, Z.; Díaz-Cruz, J.M. Enhanced voltammetric determination of metal ions by using a bismuthene-modified screen-printed electrode. *Electrochim. Acta* **2020**, *362*, 137144. [CrossRef]
28. Tapia, M.A.; Gusmão, R.; Serrano, N.; Sofer, Z.; Ariño, C.; Díaz-Cruz, J.M.; Esteban, M. Phosphorene and other layered pnictogens as a new source of 2D materials for electrochemical sensors. *TrAC—Trends Anal. Chem.* **2021**, *139*, 116249. [CrossRef]
29. Tapia, M.A.; Gusmão, R.; Pérez-Ràfols, C.; Subirats, X.; Serrano, N.; Sofer, Z.; Díaz-Cruz, J.M. Enhanced voltammetric performance of sensors based on oxidized 2D layered black phosphorus. *Talanta* **2022**, *238*, 102401. [CrossRef] [PubMed]
30. Lazanas, A.C.; Prodromidis, M.I. Electrochemical performance of passivated antimonene nanosheets and of in-situ prepared antimonene oxide-PEDOT:PSS modified screen-printed graphite electrodes. *Electrochim. Acta* **2022**, *410*, 140033. [CrossRef]
31. Lazanas, A.C.; Tsirka, K.; Paipetis, A.S.; Prodromidis, M.I. 2D bismuthene/graphene modified electrodes for the ultra-sensitive stripping voltammetric determination of lead and cadmium. *Electrochim. Acta* **2020**, *336*, 135726. [CrossRef]
32. Zhu, X.; Lin, L.; Wu, R.; Zhu, Y.; Sheng, Y.; Nie, P.; Liu, P.; Xu, L.; Wen, Y. Portable wireless intelligent sensing of ultra-trace phytoregulator α-naphthalene acetic acid using self-assembled phosphorene/Ti_3C_2-MXene nanohybrid with high ambient stability on laser induced porous graphene as nanozyme flexible electrode. *Biosens. Bioelectron.* **2021**, *179*, 113062. [CrossRef]
33. Chandra Barman, S.; Sharifuzzaman, M.; Zahed, M.A.; Park, C.; Yoon, S.H.; Zhang, S.; Kim, H.; Yoon, H.; Park, J.Y. A Highly selective and stable cationic polyelectrolyte encapsulated black phosphorene based impedimetric immunosensor for interleukin-6 biomarker detection. *Biosens. Bioelectron.* **2021**, *186*, 113287. [CrossRef] [PubMed]
34. Fatima, B.; Hussain, D.; Bashir, S.; Hussain, H.T.; Aslam, R.; Nawaz, R.; Rashid, H.N.; Bashir, N.; Majeed, S.; Ashiq, M.N.; et al. Catalase immobilized antimonene quantum dots used as an electrochemical biosensor for quantitative determination of H_2O_2 from CA-125 diagnosed ovarian cancer samples. *Mater. Sci. Eng. C* **2020**, *117*, 111296. [CrossRef] [PubMed]
35. Zhang, S.; Yan, Z.; Li, Y.; Chen, Z.; Zeng, H. Atomically Thin Arsenene and Antimonene: Semimetal-Semiconductor and Indirect-Direct Band-Gap Transitions. *Angew. Chemie—Int. Ed.* **2015**, *54*, 3112–3115. [CrossRef] [PubMed]
36. Zhang, S.; Guo, S.; Chen, Z.; Wang, Y.; Gao, H.; Gómez-Herrero, J.; Ares, P.; Zamora, F.; Zhu, Z.; Zeng, H. Recent Progress in 2D Group-VA Semiconductors: From Theory to Experiment. *Chem. Soc. Rev.* **2018**, *47*, 982–1021. [CrossRef]
37. Carrasco, J.A.; Congost-Escoin, P.; Assebban, M.; Abellán, G. Antimonene: A Tuneable Post-Graphene Material for Advanced Applications in Optoelectronics, Catalysis, Energy and Biomedicine. *Chem. Soc. Rev.* **2023**, *52*, 1288–1330. [CrossRef]

38. Ruengpirasiri, P.; Punrat, E.; Chailapakul, O.; Chuanuwatanakul, S. Graphene oxide-modified electrode coated with in-situ antimony film for the simultaneous determination of heavy metals by sequential injection-anodic stripping voltammetry. *Electroanalysis* **2017**, *29*, 1022–1030. [CrossRef]
39. Le Hai, T.; Hung, L.C.; Phuong, T.T.B.; Ha, B.T.T.; Nguyen, B.S.; Hai, T.D.; Nguyen, V.H. Multiwall carbon nanotube modified by antimony oxide (Sb2O3/MWCNTs) paste electrode for the simultaneous electrochemical detection of cadmium and lead ions. *Microchem. J.* **2020**, *153*, 104456. [CrossRef]